Longitudinal asymmetry and proton spin rotation in $\vec{p}d$ scattering with pionless effective field theory

N. Mahboubi,* S. Bayegan,† H. Nematollahi,‡ and M. Moeini Arani§
Department of Physics, University of Tehran, P.O. Box 14395-547, Tehran, Iran
(Received 25 May 2016; revised manuscript received 28 June 2016; published 15 November 2016)

The energy dependence of the longitudinal asymmetry (A_L) and the spin rotation of the proton on the deuterium target in the $\vec{p}d$ scattering are presented using the pionless effective field theory formalism. The strong, weak, and Coulomb interactions have been introduced in the $\vec{p}d$ scattering. We have shown that in the presence of Coulomb interaction, the parity-conserving (PC) and the parity-violating (PV) sectors are modified. The PV two-body transitions diagrams have been evaluated with the inclusion of Coulomb interaction and consequently the PV observables are enhanced. The leading-order values of the A_L and the spin rotation of the proton on the deuterium target are calculated at the proton laboratory energies above 0.7 MeV, in order to calculate the Coulomb effect perturbatively, up to 3 MeV where typical momenta is $Q \ll m_\pi$. With the lack of experimental data for the low-energy coupling constants (LECs), we have used two estimated sets for the five independent (PV) LECs of the weak NN PV Lagrangian. The order of magnitude, of the PV observables with these two sets, is found to be 10^{-6} to 10^{-7} which indicates that the expected order is achieved in this energy range. The cutoff independent results support the validity of our approach.

DOI: 10.1103/PhysRevC.94.054003

I. INTRODUCTION

The theoretical analysis of the nuclear parity-violation (PV) effects has been pursued in the low-energy region for the two- and three-body systems during the past 50 years. Recently, new efforts ambitiously hope to extend the calculations of the PV observables resulting from the weak interactions to few-body and complex many-body systems with lattice QCD. This is a challenging task for understanding the main features of the standard model and searching for the new physics beyond it.

The most common theoretical approach to evaluate the PV effects is based on the work of the Desplanques, Donoghue, and Holstein (DDH) potential [1]. The DDH potential has developed in terms of seven parameters representing the weak PV meson-nucleon couplings. An accurate estimate of the weak couplings is connected to the strong interaction uncertainties. For this reason the weak couplings were presented in terms of an "allowable ranges" and "best values" [2,3] based on the quark model and the symmetry arguments.

Recently evidence of the lattice QCD calculation and experiment indicates at least a factor of three below the nominal DDH "best value" for the weak meson-nucleon coupling [3]. These new evidences indicate that the DDH approach, which is based on a number of models and assumptions, may not adequately characterize the PV nucleon-nucleon (NN) interaction. These discrepancies provide motivation to focus on a model-independent parametrization of the PV effects [4].

The introduction of the model-independent and precision controlled effective field theory (EFT) provides a unified framework to calculate the nuclear PV effects in terms of the PV weak NN potentials based on two versions of EFT. These potentials were derived up to next-to-next-to-leading order (N^2LO) from the pionless and the pionful EFT Lagrangians [5]. At energies well below pion production, the nucleons and photons are the only dynamical degrees of freedom, the pionless effective field theory [EFT($\not\pi$)] is relevant to study the PV effects. Instead of calculating the PV amplitudes by potentials, we sum Feynman PV diagrams in a systematic EFT($\not\pi$). The PV two-body transition at the lowest order and the lowest energy connects an S-wave and a P-wave channel. In the EFT($\not\pi$) the PV Lagrangian depends at the leading order on five independent operators parametrized by a set of five independent and unknown S-P waves combinations of the low-energy constants (LECs) [5].

A large number of the PV effects can then be evaluated in terms of the LECs with EFT($\not\pi$). These PV effects are, in the two-body sector, the longitudinal asymmetry in the $\vec{p}p, \vec{n}n, \vec{p}n$ scatterings [6], the photon asymmetry with respect to neutron polarization and the circular polarization of the outgoing photon in the $np \to d\gamma$ [7], the energy dependence of the PV asymmetry of the circularly polarized photon in the $d\gamma \to np$ [8]. In the three-body sector: the neutron spin rotation in the hydrogen and the neutron spin rotation in the deuterium [9], the circular polarization of γ emission in the $nd \to {}^3\mathrm{H}\,\gamma$ reaction [10], beam $\vec{n}d$ and target $n\vec{d}$ asymmetries as function of the c.m. energy for the nd scattering [11], $\vec{n}d \to {}^3\mathrm{H}\,\gamma$ or $n\vec{d} \to {}^3\mathrm{H}\,\gamma$ processes [12], the energy dependence of the longitudinal asymmetry, and the proton spin rotation in the $\vec{p}d$ scattering. In this respect the calculation of the PV effect for the scattering of protons from few-nucleon ${}^2\mathrm{H}$, ${}^3\mathrm{H}$, ${}^4\mathrm{H}$ systems has to be treated perturbatively with the inclusion of the Coulomb interaction above the 0.7 proton laboratory energy. Also the range of the energies for EFT($\not\pi$) calculations and the measured PV effects must be kept below pion production in order to correctly match the theoretical calculation, in terms of LECs, to the experimental data.

*n.mahboubi@ut.ac.ir
†Corresponding author: bayegan@ut.ac.ir
‡hnematollahi.91@ut.ac.ir
§m.moeini.a@ut.ac.ir

In order to obtain information on the weak force between neutrons and protons in the three-nucleon system and due to the complexities and difficulties inherent in the different experiments in the two- and three-body sectors, the focus is on the theoretical investigation of the simplest systems for the asymmetry in the $\vec{n}d$ and $\vec{p}d$. In this paper, we have calculated the energy dependence of the longitudinal asymmetry A_L in the $\vec{p}d$ scattering [13] and the proton spin rotation on the deuteron target. We intend to use the EFT($\not\pi$) for calculating these PV observables with the inclusion of strong and Coulomb interactions for the parity-conserving (PC) and the PV amplitudes at very low energies at the leading order (LO). We have shown that in the presence of a Coulomb interaction the PV effect is modified due to diagrams connecting the different PV two-body transitions and Coulomb interaction. We obtain a prediction for A_L and the proton spin rotation in terms of different contributions multiplied by the unknown S-P wave combinations of LECs for a specific proton laboratory energy. We find that the dominant contribution to A_L and the proton spin rotation comes from the contribution which is multiplied by the $g^{^3S_1-{}^3P_1}$ low-energy constant. It is a general understanding that only $g^{^3S_1-{}^3P_1}$ make a link to the one-pion exchange coupling constant [3,5]. The prediction of the PV effects in the $\vec{n}d$ reaction has been carried out using operators from the EFT($\not\pi$) or pionful EFT potentials to calculate the matrix elements with realistic wave functions. In these evaluations of the neutron spin rotation, the contribution of the long-range part of the PV potentials is dominated due to the one-pion exchange [14,15].

To this point no experimental data for the $\vec{p}d$ or $\vec{n}d$ scattering have been reported at very low energies. The lack of five experimental measurements for the PV observables is the main obstacle to pin down the PV LECs of the LO Lagrangian. Therefore, new experimental efforts for the simple systems like $\vec{n}d$ and $\vec{p}d$ are needed to measure the PV effects and consequently constrain the LECs. In the present circumstance with no available experimental data we use two sets for the PV coefficients values. The first set is obtained by matching the five EFT($\not\pi$) relation for the PV observables A_γ^{np}, P_γ^{np}, $\frac{1}{\rho}\frac{d\phi^{np}}{dl}$, $\frac{1}{\rho}\frac{d\phi^{nd}}{dl}$, and P_γ^{nd} to the DDH "best values" estimates for these observables [12]. The second estimates for the PV LECs are introduced by a translation from LECs to the DDH parameters using the results in [11].

In this respect, the older calculation of A_L in $\vec{p}d$ scattering with the use of a phenomenological parametrization of the parity nonconservation NN interaction has been suggested 30 years ago [16]. The analysis of A_L in the $\vec{p}d$ scattering has been developed with the DDH potential [1]. The $A_L = -1.3 \times 10^{-7}$ has been estimated at 15 MeV proton laboratory energy with Danilov parameter based on DDH best values. The A_L calculation based on the Faddeev approach has been performed at 14.4 MeV for the $\vec{p}d$ scattering, A_L is reported as -1.8×10^{-7} [13]. In these theoretical efforts, the three-body interaction as well as the Coulomb effect have not been considered. The experimental data of A_L have been measured in the $\vec{p}d$ scattering at proton laboratory energies of 15 MeV at LANL [17] and for 45 MeV at PSI [18]. These experimental efforts are limited over a range of energy and do not distinguish elastic from breakup events.

In the present work, the PC pd formalism is briefly considered in Sec. II and the PV formulation for the $\vec{p}d$ scattering is introduced in terms of the unknown S-P wave combinations of LECs in Sec. III. The A_L and the proton spin rotation results are presented in Sec. IV. In Sec. V we summarize our results and present an outlook.

II. PARITY-CONSERVING *pd* SCATTERING

For calculating the A_L, we need to calculate both the PC and PV amplitudes. The interactions which are considered in the present work consist of two sectors, strong and Coulomb interactions. The PC and PV amplitudes should be calculated using these two interactions.

At the low-energy regime with tthe EFT($\not\pi$) formalism, the relevant degrees of freedom are nucleons. The expansion parameter to express the physical observables is $Q/\bar{\Lambda}$ [19,20], where Q and $\bar{\Lambda}$ are the low- and high-energy scales, respectively. The external momentums are formally considered as a Q and the pion mass is scaled as $\bar{\Lambda}$. We start by explaining briefly about the EFT($\not\pi$) interactions and power counting for the PC formalism of pd scattering which previously presented in [21,22].

The PC Lagrangian in the auxiliary field formalism for the pd system in the EFT($\not\pi$) is given by [23,24]

$$\begin{aligned}\mathcal{L}_{PC} = {} & N^\dagger\left(i\partial_0 + \frac{\nabla^2}{2m_N}\right)N + d_s^{A^\dagger}\left[\Delta_s - c_{0s}\left(i\partial_0 + \frac{\nabla^2}{4m_N} + \frac{\gamma_s^2}{m_N}\right)\right]d_s^A + d_t^{i^\dagger}\left[\Delta_t - c_{0t}\left(i\partial_0 + \frac{\nabla^2}{4m_N} + \frac{\gamma_t^2}{m_N}\right)\right]d_t^i \\ & - \left(y_s d_s^{A^\dagger}(N^\dagger P^A N) + y_t d_t^{i^\dagger}(N^\dagger P^i N) + \text{H.c.}\right) + \frac{m_N H(\Lambda)}{6}\, N^\dagger\left(y_t^2\left(d_t^i\sigma_i\right)^\dagger\left(d_t^j\sigma_j\right) - \left[y_t y_s\left(d_t^i\sigma_i\right)^\dagger\left(d_s^A\sigma_A\right) + \text{H.c.}\right]\right. \\ & \left. + y_s^2\left(d_s^A\tau_A\right)^\dagger\left(d_s^B\sigma_B\right)\right)N + \ldots, \end{aligned} \tag{1}$$

where N is the nucleon field with mass m_N. d_t^i (d_s^A) denotes spin-triplet (singlet) dibaryon field and τ_A (σ_i) represents the Pauli matrices in the isospin (spin) space. Also $y_{t,s}$ are the dibaryon-nucleon-nucleon (dNN) coupling constants. The operators $P^i = \frac{1}{\sqrt{8}}\sigma_2\sigma^i\tau_2$ and $P^A = \frac{1}{\sqrt{8}}\sigma_2\tau_2\tau^A$ a project two-nucleon state on the spin triplet and singlet channels. The LO parameters $\Delta_{s,t}$ indicate the mass differences between the ${}^1S_0$ and ${}^3S_1$ dibaryons and two-nucleon state, respectively, which are determined from the poles of the NN scattering amplitudes at $i\gamma_{s,t}$. Here γ_t is the binding momentum about

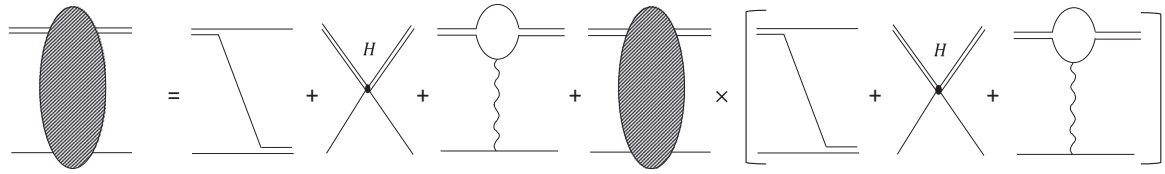

FIG. 1. The PC *pd* scattering diagrams at LO. Single line represents a nucleon. Double line is a dibaryon propagator. H shows the three-body interaction. Also, the wavy line denotes the exchanged photon. Dashed oval indicates the PC scattering amplitude.

the deuteron pole, and γ_s is the inverse of the scattering length in the $^1S_0$ channel. According to the naive dimensional analysis (NDA) the dimensionless parameters $c_{0s,t}$ first appear at the next-to-leading order (NLO), they are chosen by [23]

$$c_{0s,t} = -\frac{m_N}{2\gamma_{s,t}}\,(z_{s,t}-1), \tag{2}$$

where $z_{s,t} = \frac{1}{1-\gamma_{s,t}\rho_{s,t}}$ are written according to the effective range of the triplet and singlet systems, $\rho_{s,t}$.

The fact is that the observables must be cut-of independent, all dependencies can be removed by entering the three-body force $H(\Lambda)$ which depends on the cut-off momentum. Because of the Pauli principle, the $H(\Lambda)$ only enters in the $^2S_{\frac{1}{2}}$ (doublet) channel. At LO, the analytic form of $H(\Lambda)$ is given by [25]

$$H(\Lambda) = c \times \frac{\sin\left(s_0 \ln\left(\frac{\Lambda}{\Lambda^*}\right) + \arctan s_0\right)}{\sin\left(s_0 \ln\left(\frac{\Lambda}{\Lambda^*}\right) - \arctan s_0\right)}, \tag{3}$$

where, $c = 0.877, s_0 = 1.00624$, and $\Lambda^* = 1.55$ MeV. To calculate these coefficients, $H(\Lambda)$ is evaluated to reproduce the correct doublet S-wave nd scattering length, $a = 0.65$ fm. The PC *pd* scattering diagrams at LO are introduced in Fig. 1. The dashed oval denotes the PC *pd* scattering amplitudes at LO. The single line indicates nucleon with the propagator

$$i\Delta_N(E,q) = \frac{i}{E - \frac{q^2}{2m_N} - i\epsilon}, \tag{4}$$

and the wavy line shows the exchanged photon with the propagator

$$i\Delta_{ph}(q) = \frac{i}{q^2+\lambda^2}, \tag{5}$$

where q and λ are the momentum and mass of the exchanged photon, respectively. The small photon mass must be entered to regulate infrared divergences of the photon propagator at zero momentum transfer. To obtain well-converged results, we can extrapolate calculations to the physical case by $\lambda \to 0$ [21] (see Sec. IV).

In Fig. 1, the double line also represents the dibaryon field with the matrix propagator

$$\mathcal{D}^{(LO)}(E,q) = \begin{pmatrix} D_t^{(LO)}\left(E - \frac{q^2}{2m_N}, q\right) & 0 & 0 \\ 0 & D_s^{(LO)}\left(E - \frac{q^2}{2m_N}, q\right) & 0 \\ 0 & 0 & D_{s,pp}^{(LO)}\left(E - \frac{q^2}{2m_N}, q\right) \end{pmatrix}, \tag{6}$$

where the LO propagators of the triplet, singlet, and proton-proton (pp) parts of the $^1S_0$ dibaryon are given by

$$\begin{aligned} D_t^{(LO)}(E,q) &= \frac{4\pi}{m_N\, y_t^2}\quad \frac{1}{\gamma_t - \sqrt{\frac{q^2}{4} - m_N E - i\varepsilon}}, \\ D_s^{(LO)}(E,q) &= \frac{4\pi}{m_N\, y_s^2}\quad \frac{1}{\gamma_s - \sqrt{\frac{q^2}{4} - m_N E - i\varepsilon}}, \\ D_{s,pp}^{(LO)}(q) &= \frac{4\pi}{m_N\, y_s^2}\quad \frac{1}{\frac{1}{a_C} + \alpha m_N \tilde{H}_0(\frac{\alpha m_N}{2q'})}, \end{aligned} \tag{7}$$

respectively, with the following parameters:

$$y_s^2 = \frac{8\pi}{\rho_s\, m_N^2}, \quad y_t^2 = \frac{8\pi}{\rho_t\, m_N^2}, \tag{8}$$

$$\alpha = \frac{e^2}{4\pi} \sim \frac{1}{137}, \quad q' = i\sqrt{\frac{q^2}{4} - m_N E - i\epsilon}, \tag{9}$$

$$\tilde{H}_0(\eta) = \psi(i\eta) + \frac{1}{2i\eta} - \log(i\eta). \tag{10}$$

In the above equations, the function ψ is the logarithmic derivative of the Γ function. Also, a_c and r_c denote the scattering length and the effective range of the pp channel, respectively.

Here, we need to calculate the Faddeev equations of the diagrams in Fig. 1 for the quartet and doublet channels. The contribution of the *pd* scattering amplitude in the quartet channel has only been obtained using the $t_{q,\,t\to t}$ transition which represents the amplitude for the $pd_t \to pd_t$ transition. Thus, in the $^4S_{\frac{3}{2}}$ channel we have

$$\begin{aligned} t_{q,\,t\to t}^{(L)}(E;k,p) = -2y_{tt}\Big(K_s^{(L)}(E;k,p) - \frac{1}{2}K_c^{(L),PC}(E;k,p)\Big) \\ + \frac{y_{tt}}{\pi^2}\int_0^\Lambda d\,q\,q^2\Big(K_s^{(L)}(E;q,p) \\ - \frac{1}{2}K_c^{(L),PC}(E;q,p)\Big)\, D_t^{(LO)}\, t_{q,\,t\to t}^{(L)}(E;k,q). \end{aligned} \tag{11}$$

By using Eq. (11) the 3×1 quartet amplitude for the *pd* scattering is given

by

$$t_q^{(L)}(E;k,p)=\begin{pmatrix} t_{q,\,t\to t}^{(L)}(E;k,p)\\ 0\\ 0\end{pmatrix}. \tag{12}$$

Also, the Faddeev equation of the PC pd scattering in the doublet channel can be written as

$$\begin{aligned}\begin{pmatrix} t_{d,\,t\to t}^{(L)}\\ t_{d,\,t\to s_1}^{(L)}\\ t_{d,\,t\to s_2}^{(L)}\end{pmatrix}(E;k,p,\Lambda)&=\begin{pmatrix} y_{tt}\big(K_s^{(L)}+K_c^{(L),PC}+\delta_0^L\,\frac{2H(\Lambda)}{\Lambda^2}\big)\\ -y_{ts}\big(K_s^{(L)}+\delta_0^L\,\frac{2H(\Lambda)}{3\Lambda^2}\big)\\ -y_{ts}\big(2K_s^{(L)}+\delta_0^L\,\frac{4H(\Lambda)}{3\Lambda^2}\big)\end{pmatrix}+\frac{1}{2\pi^2}\int_0^\Lambda d\,q\,q^2\\ &\times\begin{pmatrix} -y_{tt}\big(K_s^{(L)}+K_c^{(L),PC}+\delta_0^L\,\frac{2H(\Lambda)}{\Lambda^2}\big) & y_{ts}\big(3K_s^{(L)}+\delta_0^L\,\frac{2H(\Lambda)}{\Lambda^2}\big) & y_{ts}\big(3K_s^{(L)}+\delta_0^L\,\frac{2H(\Lambda)}{\Lambda^2}\big)\\ y_{ts}\big(K_s^{(L)}+\delta_0^L\,\frac{2H(\Lambda)}{3\Lambda^2}\big) & y_{ss}\big(K_s^{(L)}-K_c^{(L),PC}-\delta_0^L\,\frac{2H(\Lambda)}{3\Lambda^2}\big) & -y_{ss}\big(K_s^{(L)}+\delta_0^L\,\frac{2H(\Lambda)}{3\Lambda^2}\big)\\ y_{ts}\big(2K_s^{(L)}+\delta_0^L\,\frac{4H(\Lambda)}{3\Lambda^2}\big) & -y_{ss}\big(2K_s^{(L)}+\delta_0^L\,\frac{4H(\Lambda)}{3\Lambda^2}\big) & -y_{ss}\,\delta_0^L\,\frac{4H(\Lambda)}{3\Lambda^2}\end{pmatrix}\\ &\times\mathcal{D}^{(LO)}(E,q)\begin{pmatrix} t_{d,\,t\to t}^{(L)}\\ t_{d,\,t\to s_1}^{(L)}\\ t_{d,\,t\to s_2}^{(L)}\end{pmatrix}(E;k,q,\Lambda),\end{aligned} \tag{13}$$

where subscripts s and c in the $K_s^{(L)}$ and $K_c^{(L),PC}$ refer to strong and Coulomb interactions and the superscript L denotes the scattering in the L-wave channel. The strong interaction kernel $K_s^{(L)}$ is

$$K_s^{(L)}(E;k,p)=\frac{1}{2}\int_{-1}^{1}d\cos\theta\quad\frac{P_L(\cos\theta)}{p^2+k^2-m_NE+kp\cos\theta}=\frac{(-1)^L}{kp}\;Q_L\Big(\frac{p^2+k^2-m_NE}{kp}\Big), \tag{14}$$

where the function Q_L is given by the relation

$$Q_L(a)=\frac{1}{2}\int_{-1}^{1}dx\quad\frac{P_L(x)}{x+a}, \tag{15}$$

and the Coulomb interaction kernel is

$$K_c^{(L),PC}(k,p)=\frac{1}{2}\int_0^\Lambda dqq^2\int_{-1}^{1}a_L^{\rm loop}[k,q,p,\theta]d\cos\theta, \tag{16}$$

for $L=0,1$ we have

$$a_{L=0}^{\rm loop}=\frac{1}{G\sqrt{F}}\Big[\ln\Big(\frac{A+B}{A-B}\Big)-\ln\Big(\frac{B(2C+D)-A(D+2E)+2\sqrt{F}\sqrt{C+E+D}}{B(2C-D)-A(D-2E)+2\sqrt{F}\sqrt{C+E-D}}\Big)\Big], \tag{17}$$

$$a_{L=1}^{\rm loop}=\cos\theta\times a_{L=0}^{\rm loop}, \tag{18}$$

with the following parameters:

$$A=-k^2-q^2+m_NE,\quad B=-kq,\quad E=k^2p^2, \tag{19}$$

$$C=(m_NE-k^2-p^2)^2-k^2q^2(1-\cos^2\theta), \tag{20}$$

$$D=-2kp\cos\theta(-k^2-p^2+m_NE), \tag{21}$$

$$G=q^2+p^2+\lambda^2-2qp\cos\theta, \tag{22}$$

$$F=B^2C+A^2E-ABD. \tag{23}$$

In Eq. (13), $t_{d,x\to y}^{(L)}$ denotes the L-wave $Nd_x\to Nd_y$ transition amplitude in the doublet channel. x,y are t, s_1, and s_2 which represent the ${}^3S_1$, ${}^1S_0$, and pp parts of ${}^1S_0$ dibaryons, respectively. We note that the constants y_{tt}, y_{ss}, and y_{ts} in the above relations are given using

$$y_{tt}=\frac{m_N\,y_t^2}{2},\quad y_{ss}=\frac{m_N\,y_s^2}{2},\quad y_{ts}=\frac{m_N\,y_t y_s}{2}. \tag{24}$$

III. PARITY-VIOLATING *pd* SCATTERING

The PV interaction connects the states with the same total angular momentums and the different parities. At the lowest order the PV interaction mixes the S-wave and P-wave channels. So, we have the ${}^3S_1\to{}^1P_1$, ${}^3S_1\to{}^3P_1$, and ${}^1S_0\to{}^3P_0$ transitions in the NN systems. Therefore, the LO Lagrangian for the two-body PV transitions can be written as

$$\begin{aligned}\mathcal{L}_{PV}=-\big[&g^{{}^3S_1-{}^1P_1}d_t^{i^\dagger}N^Ti(\overleftarrow{\nabla}\sigma_2\tau_2-\sigma_2\tau_2\overrightarrow{\nabla})_iN\\&+g_{\triangle I=0}^{{}^1S_0-{}^3P_0}d_s^{A^\dagger}N^Ti(\overleftarrow{\nabla}\sigma_2\sigma_i\tau_2\tau_A-\sigma_2\sigma_i\tau_2\tau_A\overrightarrow{\nabla})_iN\\&+g_{\triangle I=1}^{{}^1S_0-{}^3P_0}\varepsilon^{3AB}d_s^{A^\dagger}N^T(\overleftarrow{\nabla}\sigma_2\sigma_i\tau_2\tau_B-\sigma_2\sigma_i\tau_2\tau_B\overrightarrow{\nabla})_iN\\&+g_{\triangle I=2}^{{}^1S_0-{}^3P_0}\mathcal{I}^{AB}d_s^{A^\dagger}N^Ti(\overleftarrow{\nabla}\sigma_2\sigma_i\tau_2\tau_B-\sigma_2\sigma_i\tau_2\tau_B\overrightarrow{\nabla})_iN\\&+g^{{}^3S_1-{}^3P_1}\varepsilon^{ijk}d_t^{i^\dagger}N^T(\overleftarrow{\nabla}\sigma_2\sigma_k\tau_2\tau_3-\sigma_2\sigma_k\tau_2\tau_3\overrightarrow{\nabla})_jN\\&+\text{H.c.}+\ldots\big],\end{aligned} \tag{25}$$

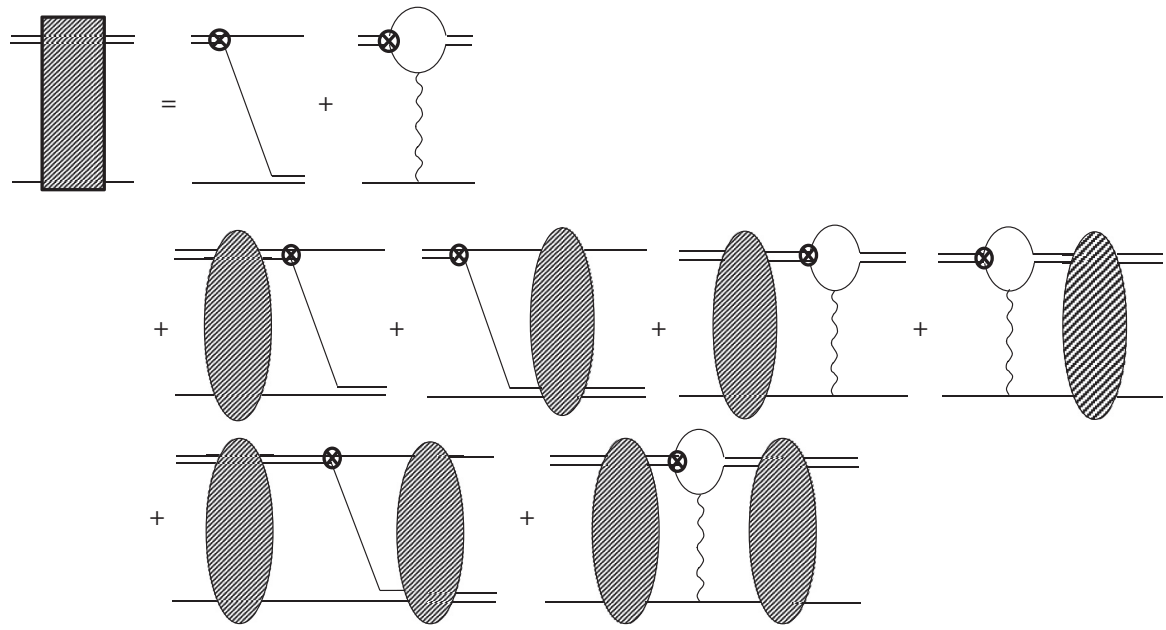

FIG. 2. The PV scattering diagrams at LO. Circle with a cross denotes the PV dNN vertex. Dashed oval indicates PC scattering amplitudes at LO. The dashed rectangular represents the PV scattering amplitude. Time-reversed diagrams are not displayed.

where $\mathcal{I} = \text{diag}(1,1,-2)$ is a diagonal matrix in the isospin space and $g^{(\overline{x}-\overline{y})}$ denotes the weak dNN coupling constant for the PV two-body transition between $\overline{x}$ and $\overline{y}$ partial waves. ΔI represents the isospin change in the PV vertex. Grießhammer *et al.* [26] show that in the PV sector the three-nucleon interaction ($3N$I) first appears at N^{2}LO, so in this paper no PV $3N$I are included. To simplify, we use the notation suggested in [10] in which $g^{^3S_1-{}^1P_1}$, $g^{^1S_0-{}^3P_0}_{\Delta I=0}$, $g^{^1S_0-{}^3P_0}_{\Delta I=1}$, $g^{^1S_0-{}^3P_0}_{\Delta I=2}$, and $g^{^3S_1-{}^3P_1}$ have been replaced by g_1, g_2, g_3, g_4, and g_5, respectively. In the LO PV the g_4 corresponding to the $g^{^1S_0-{}^3P_0}_{\Delta I=2}$ term does not contribute.

The diagrams which contribute to the LO PV pd scattering amplitude are shown in Fig. 2. In this figure, the circle with a cross indicates the PV dNN vertex. The dashed oval and rectangle represent the PC and PV scattering amplitudes, respectively.

In the cluster-configuration space, the contributions of the diagrams in Fig. 2 are obtained by

$$
\begin{aligned}
T^{LO,PV}(X\to Y,E,k,p) = {} & \mathcal{Z}^\dagger A^{PV}[X\to Y,E,k,p]\,\mathcal{Z} - \frac{1}{2\pi^2}\int_0^\Lambda dq\, q^2 \Big\{ \mathcal{Z}^\dagger A^{PV}[X\to Y,E,q,p]\,\mathcal{D}^{LO}\Big(E-\frac{q^2}{2m_N},q\Big) \\
& \times t^{LO,PC}(X,E,k,q) + t^{\dagger LO,PC}(Y,E,q,p)\,\mathcal{D}^{LO}\Big(E-\frac{q^2}{2m_N},q\Big) A^{PV}[X\to Y,E,k,q]\,\mathcal{Z}\Big\} \\
& + \frac{1}{4\pi^4}\int_0^\Lambda dq_1\, q_1^2 \int_0^\Lambda dq_2\, q_2^2 \Big\{ t^{\dagger LO,PC}(Y,E,q_2,p)\mathcal{D}^{LO}\Big(E-\frac{q_2^2}{2m_N},q_2\Big) \\
& \times A^{PV}[X\to Y,E,q_1,q_2\,]\,\mathcal{D}^{LO}\Big(E-\frac{q_1^2}{2m_N},q_1\Big) t^{LO,PC}(X,E,k,q_1)\Big\},
\end{aligned}
\tag{26}
$$

where A^{PV} represents the contributions of the first line diagrams. The second and third terms in Eq. (26) correspond to the diagrams in the second and third lines of Fig. 2. $t^{LO,PC}(X/Y;E,k,p)$ (dashed oval in Fig. 2) is the LO PC pd scattering amplitude vector for the incoming (outgoing) X (Y) partial wave. For spin $\frac{3}{2}$ and $\frac{1}{2}$, $t^{LO,PC}$ are obtained by Eqs. (12) and (13), respectively.

Note that in Eq. (26), the $\mathcal{Z}$ vector

$$
\mathcal{Z} = \begin{pmatrix} \sqrt{\mathcal{Z}_t^{LO}} \\ 0 \\ 0 \end{pmatrix}, \tag{27}
$$

with $\sqrt{\mathcal{Z}_t^{LO}}$ as the normalization factor of the deuteron wave function

$$
\mathcal{Z}_t^{LO} = \left(\frac{\partial}{\partial E} \frac{1}{D_t^{(LO)}(E,q)} \bigg|_{E=-\frac{\gamma_t^2}{m_N},q=0} \right)^{-1} = \frac{8\pi\gamma_t}{m_N^2 y_t^2}, \tag{28}
$$

is considered to obtained for the physical amplitude for pd scattering. The $A^{PV}[X\to Y,E,k,p]$ which is used in Eq. (26), is given by the relation

$$
A^{PV}[X\to Y,E,k,p] = \sum_{i=1}^{4} A_i^{PV}[X\to Y,E,k,p], \tag{29}
$$

where the A_1^{PV} and A_2^{PV} kernels are for the contributions of the first and second diagrams in line 1 of Fig. 2. Also, the time-reversed amplitudes of these diagrams (not shown in Fig. 2) are introduced by A_3^{PV} and A_4^{PV}, respectively. The $A_{1,2}^{PV}$ functions for all the possible transitions in the $J=\frac{1}{2}$ channels are given by

$$A_1^{PV}\left[{}^2S_{\frac{1}{2}} \to {}^2P_{\frac{1}{2}}; E,k,p\right] = \frac{\sqrt{2}m_N y_t}{4kp}[kQ_1(\varepsilon)+2pQ_0(\varepsilon)]\begin{pmatrix} 3g_1+2g_5 & -g_2 & -2g_2-2g_3 \\ g_1-2g_5 & g_2 & -2g_2 \\ 2g_1-4g_5 & -2g_2 & 0 \end{pmatrix}, \tag{30}$$

$$A_1^{PV}\left[{}^2P_{\frac{1}{2}} \to {}^2S_{\frac{1}{2}}; E,k,p\right] = \frac{\sqrt{2}m_N y_t}{4kp}[2pQ_1(\varepsilon)+kQ_0(\varepsilon)]\begin{pmatrix} 3g_1+2g_5 & -g_2 & -2g_2-2g_3 \\ g_1-2g_5 & g_2 & -2g_2 \\ 2g_1-4g_5 & -2g_2 & 0 \end{pmatrix}, \tag{31}$$

$$A_1^{PV}\left[{}^2S_{\frac{1}{2}} \to {}^4P_{\frac{1}{2}}; E,k,p\right] = \frac{m_N y_s}{kp}[kQ_1(\varepsilon)+2pQ_0(\varepsilon)]\begin{pmatrix} g_5 & g_2 & 2g_2+2g_3 \\ 0 & 0 & 0 \\ 0 & 0 & 0 \end{pmatrix}, \tag{32}$$

$$A_1^{PV}\left[{}^4P_{\frac{1}{2}} \to {}^2S_{\frac{1}{2}}; E,k,p\right] = \frac{m_N y_t}{2kp}[2pQ_1(\varepsilon)+kQ_0(\varepsilon)]\begin{pmatrix} 3g_1-g_5 & 0 & 0 \\ g_1+g_5 & 0 & 0 \\ 2g_1+2g_5 & 0 & 0 \end{pmatrix}, \tag{33}$$

$$A_2^{PV}\left[{}^2S_{\frac{1}{2}} \to {}^2P_{\frac{1}{2}}; E,k,p\right] = \frac{\sqrt{2}m_N e^2 y_t}{16\pi^2}\left[kK_c^{(1),PC}(k,p)+2K_c^{(0),PV}(k,p)\right]\begin{pmatrix} 2g_5 & -g_2 & 0 \\ -g_1 & 0 & 0 \\ 0 & 0 & 0 \end{pmatrix}, \tag{34}$$

$$A_2^{PV}\left[{}^2P_{\frac{1}{2}} \to {}^2S_{\frac{1}{2}}; E,k,p\right] = \frac{\sqrt{2}m_N e^2 y_t}{16\pi^2}\left[2K_c^{(1),PV}(k,p)+kK_c^{(0),PC}(k,p)\right]\begin{pmatrix} 2g_5 & -g_2 & 0 \\ -g_1 & 0 & 0 \\ 0 & 0 & 0 \end{pmatrix}, \tag{35}$$

$$A_2^{PV}\left[{}^2S_{\frac{1}{2}} \to {}^4P_{\frac{1}{2}}; E,k,p\right] = \frac{m_N e^2 y_s}{8\pi^2}\left[kK_c^{(1),PC}(k,p)+2K_c^{(0),PV}(k,p)\right]\begin{pmatrix} -g_5 & -g_2 & 0 \\ 0 & 0 & 0 \\ 0 & 0 & 0 \end{pmatrix}, \tag{36}$$

$$A_2^{PV}\left[{}^4P_{\frac{1}{2}} \to {}^2S_{\frac{1}{2}}; E,k,p\right] = \frac{m_N e^2 y_t}{8\pi^2}\left[2K_c^{(1),PV}(k,p)+kK_c^{(0),PC}(k,p)\right]\begin{pmatrix} -g_5 & 0 & 0 \\ -g_1 & 0 & 0 \\ 0 & 0 & 0 \end{pmatrix}. \tag{37}$$

Also, for the $J=\frac{3}{2}$ we have

$$A_1^{PV}\left[{}^4S_{\frac{3}{2}} \to {}^2P_{\frac{3}{2}}; E,k,p\right] = \frac{\sqrt{2}m_N y_t}{4kp}[kQ_1(\varepsilon)+2pQ_0(\varepsilon)]\begin{pmatrix} 3g_1-g_5 & 0 & 0 \\ g_1+g_5 & 0 & 0 \\ 2g_1+2g_5 & 0 & 0 \end{pmatrix}Q_s^r, \tag{38}$$

$$A_1^{PV}\left[{}^2P_{\frac{3}{2}} \to {}^4S_{\frac{3}{2}}; E,k,p\right] = \frac{\sqrt{2}m_N y_s}{2kp}[2pQ_1(\varepsilon)+kQ_0(\varepsilon)]\begin{pmatrix} g_5 & g_2 & 2g_2+2g_3 \\ 0 & 0 & 0 \\ 0 & 0 & 0 \end{pmatrix}Q_s^r, \tag{39}$$

$$A_1^{PV}\left[{}^4S_{\frac{3}{2}} \to {}^4P_{\frac{3}{2}}; E,k,p\right] = \frac{\sqrt{10}m_N y_s}{2kp}[kQ_1(\varepsilon)+2pQ_0(\varepsilon)]\begin{pmatrix} g_5 & 0 & 0 \\ 0 & 0 & 0 \\ 0 & 0 & 0 \end{pmatrix}Q_s^r, \tag{40}$$

$$A_1^{PV}\left[{}^4P_{\frac{3}{2}} \to {}^4S_{\frac{3}{2}}; E,k,p\right] = \frac{\sqrt{10}m_N y_s}{2kp}[2pQ_1(\varepsilon)+kQ_0(\varepsilon)]\begin{pmatrix} g_5 & 0 & 0 \\ 0 & 0 & 0 \\ 0 & 0 & 0 \end{pmatrix}Q_s^r, \tag{41}$$

$$A_2^{PV}\left[{}^4S_{\frac{3}{2}} \to {}^2P_{\frac{3}{2}}; E,k,p\right] = \frac{\sqrt{2}m_N e^2 y_t}{16\pi^2}\left[kK_c^{(1),PC}(k,p)+2K_c^{(0),PV}(k,p)\right]\begin{pmatrix} -g_5 & 0 & 0 \\ -g_1 & 0 & 0 \\ 0 & 0 & 0 \end{pmatrix}Q_s^r, \tag{42}$$

$$A_2^{PV}\left[{}^2P_{\frac{3}{2}} \to {}^4S_{\frac{3}{2}}; E,k,p\right] = \frac{\sqrt{2}m_N e^2 y_s}{16\pi^2}\left[2K_c^{(1),PV}(k,p)+kK_c^{(0),PC}(k,p)\right]\begin{pmatrix} -g_5 & -g_2 & 0 \\ 0 & 0 & 0 \\ 0 & 0 & 0 \end{pmatrix}Q_s^r, \tag{43}$$

$$A_2^{PV}\left[{}^4S_{\frac{3}{2}} \to {}^4P_{\frac{3}{2}}; E,k,p\right] = \frac{\sqrt{10}m_N e^2 y_s}{16\pi^2}\left[kK_c^{(1),PC}(k,p) + 2K_c^{(0)PV}(k,p)\right]\begin{pmatrix} g_5 & 0 & 0 \\ 0 & 0 & 0 \\ 0 & 0 & 0 \end{pmatrix} Q_s^r, \tag{44}$$

$$A_2^{PV}\left[{}^4P_{\frac{3}{2}} \to {}^4S_{\frac{3}{2}}; E,k,p\right] = \frac{\sqrt{10}m_N e^2 y_s}{16\pi^2}\left[2K_c^{(1),PV}(k,p) + kK_c^{(0),PC}(k,p)\right]\begin{pmatrix} g_5 & 0 & 0 \\ 0 & 0 & 0 \\ 0 & 0 & 0 \end{pmatrix} Q_s^r \tag{45}$$

with $\varepsilon = \frac{p^2+q^2-m_N E}{pq}$. The $(Q_s^r)_\beta^\alpha = \delta_s^r\delta_\beta^\alpha - \frac{1}{3}(\sigma^r\sigma^s)_\beta^\alpha$ is the projection operator of the quartet channel. The index $r\,(s)$ is the spin component of the outgoing (incoming) ${}^3S_1$ dibaryon and $\alpha\,(\beta)$ is the spin of the outgoing (incoming) nucleon. The $K_c^{(L),PV}$ corresponds to the Coulomb interaction, where L refers to scattering in the L-wave channel. It is defined as

$$K_c^{(L),PV}(k,p) = \frac{1}{2}\int_0^\Lambda dqq^3\int_{-1}^1 a_L^{\text{loop}}[k,q,p,\theta]d\cos\theta. \tag{46}$$

The contributions of the time-reversed diagrams of the first and second ones in line 1 of Fig. 2 can be given by the relations

$$A_3^{PV}(X \to Y,E,k,p)_{s\beta}^{r\alpha} = \left[A_1^{PV}(Y \to X,E,p,k)_{r\alpha}^{s\beta}\right]^\dagger,$$
$$A_4^{PV}(X \to Y,E,k,p)_{s\beta}^{r\alpha} = \left[A_2^{PV}(Y \to X,E,p,k)_{r\alpha}^{s\beta}\right]^\dagger. \tag{47}$$

IV. NUMERICAL RESULTS OF LONGITUDINAL ANALYZING POWER AND PROTON SPIN ROTATION

In this section, we focus on the calculation of the longitudinal asymmetry of the polarized proton A_L and the spin rotation $\frac{1}{N}\frac{d\phi}{dz}$ in the $\vec{p}d$ scattering process at the LO which are defined by the relations

$$A_L = \frac{\text{Im}(f_+ - f_-)}{\text{Im}(f_+ + f_-)}, \tag{48}$$

$$\frac{1}{N}\frac{d\phi}{dz} = \frac{4m_N N}{9k}\text{Re}(f_+ - f_-) \tag{49}$$

where $f_+(f_-)$ is the elastic scattering amplitude at zero angle for the protons with the positive (negative) helicity. N is the number of scattering centers per unit volume and k is the momentum of the proton in the c.m. system.

By using Feynman diagrams, PC and PV Lagrangians, we calculate the $\vec{p}d$ scattering amplitudes. The values of g_i, which are used in this paper, are based on the evaluation by Moeini Arani [12] and Vanasse [8].

In terms of PC and PV amplitudes, the equation for A_L is given by [14]

$$\begin{aligned} A_L = \tfrac{1}{3}\text{Re}\big[&T^{LO,PV}\left({}^2P_{\frac{1}{2}} \to {}^2S_{\frac{1}{2}}\right) + T^{LO,PV}\left({}^2S_{\frac{1}{2}} \to {}^2P_{\frac{1}{2}}\right) - 2\sqrt{2}\,T^{LO,PV}\left({}^4P_{\frac{1}{2}} \to {}^2S_{\frac{1}{2}}\right) - 2\sqrt{2}\,T^{LO,PV}\left({}^2S_{\frac{1}{2}} \to {}^4P_{\frac{1}{2}}\right) \\ &- 4\,T^{LO,PV}\left({}^2P_{\frac{3}{2}} \to {}^4S_{\frac{3}{2}}\right) - 4\,T^{LO,PV}\left({}^4S_{\frac{3}{2}} \to {}^2P_{\frac{3}{2}}\right) - 2\sqrt{5}\,T^{LO,PV}\left({}^4P_{\frac{3}{2}} \to {}^4S_{\frac{3}{2}}\right) - 2\sqrt{5}T^{LO,PV}\left({}^4S_{\frac{3}{2}} \to {}^4P_{\frac{3}{2}}\right)\big] \\ &\div \text{Re}\big[T^{LO,PC}({}^2S_{\frac{1}{2}}) + 2\,T^{LO,PC}({}^4S_{\frac{3}{2}})\big], \end{aligned} \tag{50}$$

and the relation for $\frac{1}{N}\frac{d\phi}{dz}$ is introduced by [9]

$$\begin{aligned} \frac{1}{N}\frac{d\phi}{dz} = \frac{4m_N}{27k}\text{Re}\big[&T^{LO,PV}\left({}^2P_{\frac{1}{2}} \to {}^2S_{\frac{1}{2}}\right) + T^{LO,PV}\left({}^2S_{\frac{1}{2}} \to {}^2P_{\frac{1}{2}}\right) - 2\sqrt{2}\,T^{LO,PV}\left({}^4P_{\frac{1}{2}} \to {}^2S_{\frac{1}{2}}\right) \\ &- 2\sqrt{2}\,T^{LO,PV}\left({}^2S_{\frac{1}{2}} \to {}^4P_{\frac{1}{2}}\right) - 4\,T^{LO,PV}\left({}^2P_{\frac{3}{2}} \to {}^4S_{\frac{3}{2}}\right) - 4\,T^{LO,PV}\left({}^4S_{\frac{3}{2}} \to {}^2P_{\frac{3}{2}}\right) \\ &- 2\sqrt{5}\,T^{LO,PV}\left({}^4P_{\frac{3}{2}} \to {}^4S_{\frac{3}{2}}\right) - 2\sqrt{5}T^{LO,PV}\left({}^4S_{\frac{3}{2}} \to {}^4P_{\frac{3}{2}}\right)\big]. \end{aligned} \tag{51}$$

In above equations, the $T^{LO,PC}({}^2S_{\frac{1}{2}})$ and $T^{LO,PC}({}^4S_{\frac{3}{2}})$ are the normalized PC pd scattering amplitudes in the doublet and quartet channels, respectively. They are given by

$$T^{LO,PC}\left({}^2S_{\frac{1}{2}}\right) = \mathcal{Z}^\dagger\begin{pmatrix} t_{d,t\to t}^{(L)} \\ t_{d,t\to s_1}^{(L)} \\ t_{d,t\to s_2}^{(L)} \end{pmatrix}, \tag{52}$$

and

$$T^{LO,PC}\left({}^4S_{\frac{3}{2}}\right) = \mathcal{Z}^\dagger\, t_q^{(L)}. \tag{53}$$

In Table I we have presented the results of A_L at the proton laboratory energies from 0.7 to 3 MeV with different cutoffs from 200 to 900 MeV based on [12]. These results show that in the presence of the Coulomb interaction in addition to the modified PC amplitude, the PV amplitude is changed due to the diagrams connecting different PV two-body transitions and

TABLE I. Our EFT($\not\pi$) results for the A_L at the proton laboratory energies from 0.7 to 3 MeV with different cutoff momentums based on [12]. The first row indicates the cutoff and the first column shows the proton energy. Note that the results of A_L are presented in 10^{-6} unit. The numbers in the parentheses in the fourth column indicate the results for A_L when the Coulomb effect is switched off.

$E_{\rm lab}$ \ Λ	200	400	600	800	900
0.7	−13.10	−13.12	−13.14 (−11.35)	−13.17	−13.20
1.2	−9.53	−9.54	−9.55 (−8.97)	−9.57	−9.57
1.6	−8.89	−8.90	−8.91 (−7.61)	−8.93	−8.94
2.1	−8.11	−8.12	−8.13 (−6.68)	−8.15	−8.17
2.6	−7.56	−7.57	−7.58 (−5.82)	−7.60	−7.62
3	−6.68	−6.70	−6.70 (−5.74)	−6.73	−6.76

Coulomb interaction. The results of A_L for $\Lambda = 600$ MeV when the Coulomb interaction in the PC and PV sectors are switched off, are also presented in the fourth column of Table I by the numbers inside the parentheses.

To obtain the well-converged results, which are listed in Table I, we have extrapolated the calculations to $\lambda \to 0$. Figure 3 represents the comparison between the results of A_L according to the photon mass, e.g., the proton laboratory energy of 1.2 MeV and $\Lambda = 600$ MeV. Dotted line represents the results with extrapolation and the dashed line indicates the results without extrapolation method. The error introduced by the extrapolation to $\lambda \to 0$ compared to the EFT theoretical error is negligible.

Table II indicates the results for $\frac{1}{N}\frac{d\phi}{dz}$ and A_L based on two sets of g_i [8,12] at $\Lambda = 600$ MeV. The values obtained for the A_L and the proton spin rotation by the first set of LECs [12] indicate roughly a factor of one to two larger than those found by the second set [8]. We emphasize that these values are only the order of magnitude estimates. We have also noticed that the sign of A_L using these two sets is different and this is an

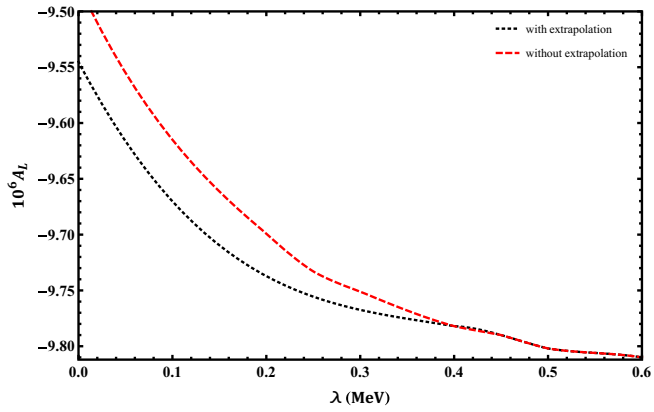

FIG. 3. The variation of A_L according to photon mass for the proton laboratory energy of 1.2 MeV and $\Lambda = 600$ MeV based on the estimated values of g_i's in [12]. Dotted line represents the results with extrapolation and the dashed line indicates the results without extrapolation method.

TABLE II. The EFT($\not\pi$) results for the $\frac{1}{N}\frac{d\phi}{dz}$ and A_L based on two sets of g_i [8,12] at the proton laboratory energies from 0.7 to 3 MeV at $\Lambda = 600$. The results are presented in 10^{-6} unit.

$E_{\rm lab}$	$\frac{1}{N}\frac{d\phi}{dz}$ [12]	A_L [12]	$\frac{1}{N}\frac{d\phi}{dz}$ [8]	A_L [8]
0.7	16.41	−13.14	−0.50	0.23
1.2	6.88	−9.54	0.32	0.35
1.6	4.32	−8.91	0.065	0.49
2.1	4.59	−8.12	0.009	0.54
2.6	−0.04	−7.57	0.0014	0.62
3	−0.07	−6.70	0.0012	0.73

TABLE III. Contribution of each g_i [12] for the calculation of A_L and $\frac{1}{N}\frac{d\phi}{dz}$ at $\Lambda = 600$ and $E_{\rm lab} = 3$ MeV in MeV$^{\frac{3}{2}}$ unit.

g_i [12]	A_L	$\frac{1}{N}\frac{d\phi}{dz}$
1	−3884.89	2.35
2	−957.53	11.08
3	−879.66	−11.12
5	−3968.99	−55.11

TABLE IV. The results for the cutoff variation of A_L between $\Lambda = 200$ and 600 MeV based on the estimated values of g_i's in [12].

$E_{\rm lab}$	0.7	1.2	1.6	2.1	2.6	3
Abs$[1 - \frac{A_L(\Lambda=200)}{A_L(\Lambda=600)}]$	0.0030	0.0020	0.0022	0.0024	0.0026	0.0029

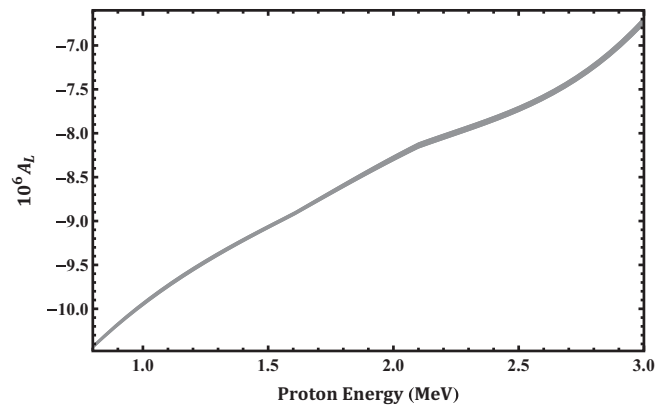

FIG. 4. A_L variation according to the proton laboratory energies from 0.8 to 3 MeV based on the estimated values of g_i's in [12].

interesting prediction. The future experimental results of $\vec{p}d$ scattering can be used to assess the estimation of the PV effects by these two sets of LECs.

The results of A_L and $\frac{1}{N}\frac{d\phi}{dz}$ in terms of their contributions for each of the g_i [12] are given in Table III. These results are given with $\Lambda = 600$ MeV and for the proton laboratory energy of 3 MeV. We see from Table III that the dominant contributions of observables comes from the $g_5 = g^{3S_1 - {}^3P_1}$ LEC which contains the one-pion exchange contribution.

The A_L variation according to the proton laboratory energies from 0.8 to 3 MeV based on [12] has been presented in Fig. 4. The thickness of the plot indicates the cutoff variation, which runs from 200 to 900 MeV. The results of the cutoff variation for A_L between $\Lambda = 200$ and 600 MeV based on the estimated values of g_i's in [12] are also shown in Table IV. These results show that our calculation is cutoff-independent and properly renormalized.

V. CONCLUSION AND OUTLOOK

In the present paper we have calculated the energy dependence of the longitudinal analyzing power in the $\vec{p}d$ scattering and the proton spin rotation with the EFT($\not\pi$). We have carried out our evaluation of the Coulomb interaction for proton-proton scattering perturbatively and typical momenta $Q \ll m_\pi$. In the presence of the Coulomb interaction the PV observables are enhanced. There is no cutoff dependence observed between 200 and 900 MeV cutoff values. In the PC sector the three-body force is introduced for pd scattering, however, no new three-body force is added in the LO PV calculation in the PV sector. The values of A_L are in the expected order and further experimental research for $\vec{p}d$ scattering would be an important laboratory effort to be carried out in the very low energies. These future experimental results of $\vec{p}d$ scattering would help to pin down the LECs and also to distinguish between the present estimates of LECs.

One could further investigate asymmetries from the photo-disintegration of ^{3}He using circularly polarized photons and the $\vec{p}d \to {}^3\text{He}\,\gamma$ processes with the EFT($\not\pi$) approach in the future. Finally, the EFT approach as a model-independent framework with new experimental efforts could prove to be a major improvement with powerful capability over model-dependent approaches.

[1] B. Desplanques, J. F. Donoghue, and B. R. Holstein, Ann. Phys. (NY) **124**, 449 (1980).
[2] B. R. Holstein, Fizika B **14**, 165 (2005).
[3] W. C. Haxton and B. R. Holstein, Prog. Part. Nucl. Phys. **71**, 185 (2013).
[4] S.-L. Zhu *et al.*, Nucl. Phys. A **748**, 435 (2005).
[5] M. R. Schindler and R. P. Springer, Prog. Part. Nucl. Phys. **72**, 1 (2013).
[6] D. R. Phillips, M. R. Schindler, and R. P. Springer, Nucl. Phys. A **822**, 1 (2009).
[7] J. W. Shin, S. Ando, and C. H. Hyun, Phys. Rev. C **81**, 055501 (2010).
[8] J. Vanasse and M. R. Schindler, Phys. Rev. C **90**, 044001 (2014).
[9] H. W. Grießhammer, M. R. Schindler, and R. P. Springer, Eur. Phys. J. A **48**, 7 (2012).
[10] M. M. Arani and S. Bayegan, Eur. Phys. J. A **49**, 117 (2013).
[11] J. Vanasse, Phys. Rev. C **86**, 014001 (2012).
[12] M. M. Arani and S. Bayegan, Few-Body Syst. **55**, 1099 (2014).
[13] W. M. Kloet, B. F. Gibson, G. J. Stephenson, and E. M. Henley, Phys. Rev. C **27**, 2529 (1983).
[14] Y. H. Song, R. Lazauskas, and V. Gudkov, Phys. Rev. C **83**, 015501 (2011).
[15] R. Schiavilla, M. Viviani, L. Girlanda, A. Kievsky, and L. E. Marcucci, Phys. Rev. C **78**, 014002 (2008).
[16] B. Desplanques and J. Missimer, Nucl. Phys. A **300**, 286 (1978); B. Desplanques, Phys. Rep. **297**, 1 (1998).
[17] J. M. Potter *et al.*, Phys. Rev. Lett. **33**, 1307 (1947); D. E. Nagle *et al.*, AIP Conf. Proc. **51**, 224 (1978).
[18] M. Simonius, in *Future Directions in Particle and Nuclear Physics at Multi-Gev Hadron Beam Facilities*, edited by D. F. Geesaman, Brookhaven National Laboratory Report No. BNL-52389 (1993), p. 147.
[19] J. W. Chen, G. Rupak, and M. J. Savage, Nucl. Phys. A **653**, 386 (1999).
[20] D. B. Kaplan, M. J. Savage, and M. B. Wise, Phys. Lett. B **424**, 390 (1998); Nucl. Phys. B **534**, 329 (1998).
[21] G. Rupak and X. Kong, Nucl. Phys. A **717**, 73 (2003).
[22] S. König, H. W. Grießhammer, and H.-W. Hammer, J. Phys. G: Nucl. Part. Phys. **42**, 045101 (2015).
[23] H. W. Grießhammer, Nucl. Phys. A **744**, 192 (2004).
[24] D. R. Phillips, G. Rupak, and M. J. Savage, Phys. Lett. B **473**, 209 (2000).
[25] J. Vanasse, D. A. Egolf, J. kerin, S. König, and R. P. Springer, Phys. Rev. C **89**, 064003 (2014).
[26] H. W. Grießhammer and M. R. Schindler, Eur. Phys. J. A **46**, 73 (2010).